

Immunoinformatics-Aided Design and *In Vivo* Validation of a Peptide-Based Multiepitope Vaccine Targeting Canine Circovirus

Published as part of the ACS Pharmacology & Translational Science virtual special issue “*New Drug Modalities in Medicinal Chemistry, Pharmacology, and Translational Science*”.

Vikas Kaushik, Pankaj Jain, Nahid Akhtar, Amit Joshi, Lovi Raj Gupta, Ravneet Kaur Grewal, Romina Oliva, Abdul Rajjak Shaikh,* Luigi Cavallo,* and Mohit Chawla*



Cite This: <https://doi.org/10.1021/acsptsci.2c00130>



Read Online

ACCESS |

Metrics & More

Article Recommendations

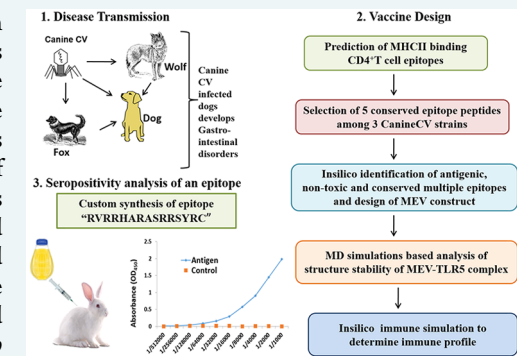
Supporting Information

ABSTRACT: Canine circovirus (CanineCV) is a deadly pathogen affecting both domestic and wild carnivores including dogs. No vaccine against CanineCV is available commercially or under clinical trials. In the present study, we have designed a promising multiepitope vaccine (MEV) construct targeting multiple strains of CanineCV. A total of 545 MHCII binding CD4⁺T cell epitope peptides were predicted from the capsid and replicase protein from each strain of CanineCV. Five conserved epitope peptides among the three CanineCV strains were selected. The final vaccine was constructed using antigenic, nontoxic, and conserved multiple epitopes identified *in silico*. Further, molecular docking and molecular dynamics simulations predicted stable interactions between the predicted MEV and canine receptor TLR-5. To validate antigenicity and immunogenicity, one of the mapped epitope peptides was synthesized. *In vivo* analysis of the selected epitope clearly indicates CD4⁺T-cell-dependent generation of antibodies which further suggests that the designed MEV construct holds promise as a candidate for vaccine against CanineCV.

KEYWORDS: immunoinformatics, canine circovirus, MD simulations, multiepitope vaccine, molecular docking

Canine circovirus (CanineCV) is a nonenveloped, covalently closed, circular single-stranded DNA virus belonging to the family Circoviridae.^{1,2} The genome of CanineCV consists of 2 kb nucleotides containing two major open reading frames as follows: (a) ORF1 (rep gene) encoding replicase for viral replication; (b) ORF2 (cap gene) encoding the capsid that participates in the host immune response.^{1,2} CanineCV is genetically close to porcine circovirus and is considered to be the first nonporcine mammalian circovirus identified from the serum of dogs.¹

Since the first evidence of CanineCV was reported, the virus has been identified in the serum, tissue, and fecal samples of dogs diagnosed with the gastroenteritis and respiratory diseases in many countries.^{2–9} Intriguingly, CanineCV is reported in healthy dogs from rural as well as the urban areas.^{9,10} Further, there is evidence which clearly suggests that CanineCV-diagnosed dogs having gastrointestinal problems are found to be co-infected with other viral strains, viz., parvovirus, vesivirus, and astrovirus.^{3,6,7,11,12} Interestingly, CanineCV is found to act synergistically with other enteric viruses, for instance, parvovirus in developing gastrointestinal disorders in the dog.^{3,6} A recent report asserted that the CanineCV-infected dogs harboring canine parvovirus-2 (CPV-2) have a high



mortality rate as compared to a dog infected with CPV-2 only.¹¹ Immunosuppression and lymphoid depletion may occur in CanineCV-infected dogs as seen with other circoviral infections; however, its pathogenesis is poorly understood.⁸

Apart from dogs, CanineCV is also found in tissue samples collected from other canines including red fox, arctic fox, and wolves in Norway and Italy.^{13,14} The existence of CanineCV in wild animals implies an impending threat to the conservation of vulnerable wild species which may also act as a potential source of infection to the dogs.¹⁵ Thus, it is imperative to search for novel avenues to control the spread of CanineCV infection in canines, especially dogs.

With the recent progress in the field of bioinformatics, different strategies have been employed to design knowledge-based vaccines using the immunoinformatics approach.^{16–21} In fact, multiepitope vaccines (MEVs) have been designed for Epstein–Barr and *Chlamydia trachomatis* viruses using immunoinformatics, which are found to elicit effective humoral and cellular responses both *in vitro* and *in vivo* (18–20). Using

Received: July 3, 2022

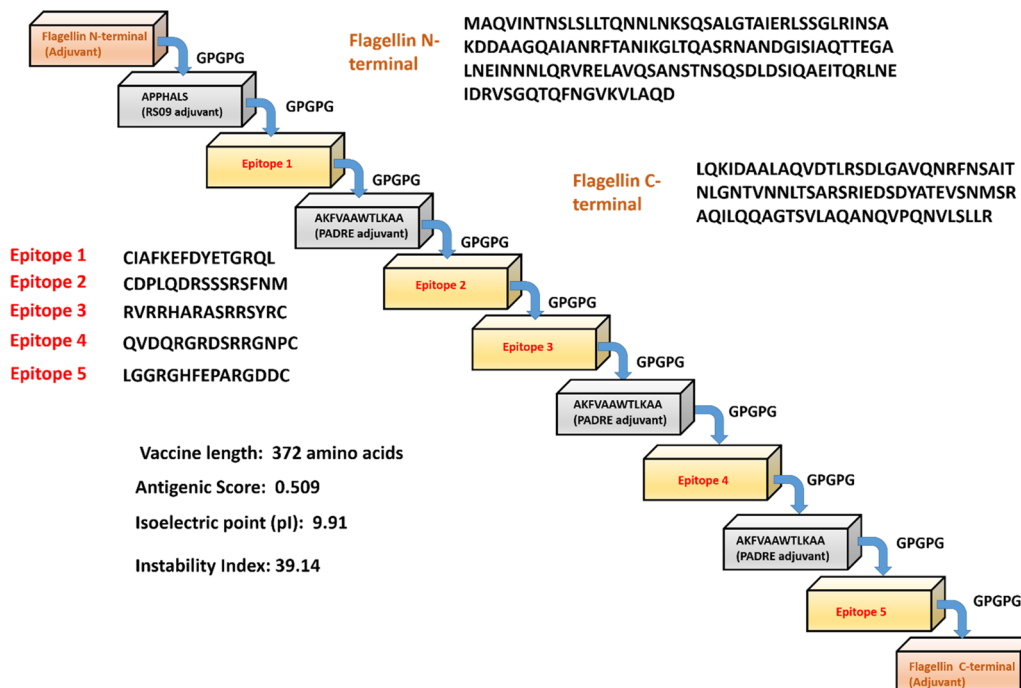


Figure 1. Schematic representation of the predicted multiepitope vaccine (MEV) construct for CanineCV with different adjuvants, linkers, and epitopes with their respective amino acid sequences.

a similar approach, we recently identified five epitopes, i.e., YQHLPPFRF, YIRAKWINW, ALYRRLTII, HLQGFVNKL, and GTMNFVARR, from capsid and replicase proteins, which could be used to design a vaccine candidate for CanineCV.²² This revelation encouraged us to envisage the vaccine development against CanineCV by targeting these two major ORFs while taking into account the distinct strains of CanineCV. In the present study, we aimed at identifying CD4⁺T cell antigenic epitopes which could stimulate B cells to generate robust and longer-lived antibody responses.²³ First, we identified highly antigenic, nonallergic, and nontoxic peptides from capsid and replicase proteins, followed by sequence conservancy analysis among the chosen strains of CanineCV. The final designed vaccine comprised all prioritized epitopes, which were fused together using suitable linkers and adjuvants for inciting an optimal immune response. Further, we thoroughly evaluated structural, immunogenic, and physicochemical (viz., stability, isoelectric point, molecular weight, and aliphatic index) parameters for the designed MEV. The binding affinity of the MEV construct toward the canine Toll-like receptor-5 (TLR-5) was evaluated by molecular docking, which was further ascertained by molecular dynamics (MD) simulations to confirm the stability of the MEV construct and of associated interactions. Further, the immune simulations have been carried out using the C-IMMSIM server. In order to establish the immunogenic potential of the peptides identified by *in silico* studies, one of the potential antigenic peptides was synthesized and used to immunize New Zealand rabbit to validate the antigenicity and immunogenicity of the selected peptide.

METHODS

2.1. Protein Sequence Retrieval. The sequence of the CanineCV proteins, i.e., the capsid and replicase, were obtained from the NCBI GenBank with accession numbers QBQ20241.1 and QFU80922.1, respectively, in FASTA

format. These sequences were considered in our previous studies as well.²² However, in the present study, we added three new protein sequences of the CanineCV capsid and replicase from three distinct strains from different continents, i.e., from China, the United States, and Germany: CanineCV strain XF16 (China), CanineCV strain OH19098-1 (U.S.A.), and CanineCV strain FUBerlin-JRS (Germany). The accession numbers for the replicase and capsid are AVT56110.1, AWN93250.1, and ALG63389.1 and AVT56111.1, AWN93251.1, and ALG63390.1, respectively. The multiple sequence alignment for the three novel strains considered in the present study along with the strain investigated in the previous work for both the capsid and replicase proteins clearly indicates the high sequence identity (i.e., >94%) among the chosen strains from different regions; see Tables S1 and S2.

2.2. Antigenicity, Toxicity, Conservancy, and IFN- γ Analysis. The epitope screening analysis was carried out by the NetMHCIIpan 4.0 server^{24,25} which allows epitope prediction based on a neural network approach. After the protein sequences had been subjected to the NetMHCIIpan server a total of 289 epitopes from the replicase and 256 epitopes from the capsid for each strain were identified. Further, conservancy and antigenicity analyses were conducted. In order to validate the results of the predicted epitopes obtained by the NetMHCIIpan server, an independent approach employing the Genscript OptimumAntigen design tool was also used. This tool employs a high-end algorithm to search various protein databases to design epitopes with the desired antigenicity and specificity. The algorithm considers various parameters such as sequence length, secondary structure regions, surface orientation, hydrophobicity/hydrophilicity, and avoidance of sequence motifs such as GTP binding sites, the RGD motif, and SH2 domains while predicting the antigenic epitopes (see the Supporting Information). An extra cysteine is added to either the N-terminus or C-terminus for the identified epitopes in

order to facilitate conjugation while predicting the antigens using the OptimumAntigen design tool. For conservancy analysis of the predicted epitopes, the IEDB epitope conservancy tool was used for CanineCV strain XF16 (China), CanineCV strain OH19098-1 (U.S.A.), and CanineCV strain FUBerlin-JRS (Germany). For these chosen strains of CanineCV, the accession numbers are AVTS6110.1, AWN93250.1, and ALG63389.1 for the replicase and AVTS6111.1, AWN93251.1, and ALG63390.1 for the capsid, respectively. Finally, the IFN epitope server was used for interferon- γ inducing ability analysis of the predicted epitopes.²⁶

2.3. Vaccine Engineering and Determination of Its Physiochemical Properties. After the selection of suitable epitopes from the capsid and replicase proteins of CanineCV the final MEV construct was designed. A GPGPG sequence was used as a linker to join RS09 and flagellin adjuvants with the selected epitopes.²³ The Pan DR epitope (PADRE) sequence was also added to improve the immunogenicity as well as the stability of the CanineCV vaccine construct.²⁴ The final designed MEV construct is shown in Figure 1. The ExPASy ProtParam web server was used to predict the physiochemical properties such as stability, isoelectric point, molecular weight, and aliphatic index as well as several other properties of the MEV construct.²⁷ The antigenicity of the predicted MEV construct was also analyzed by the VaxiJen web server.²⁸ This server predicts the antigenicity of viral, fungal, tumor, or bacterial peptide sequences on the basis of their physiochemical properties.²⁹ Further, the ToxinPred server was used for toxicity analysis.³⁰ The ToxinPred web server can predict the toxicity of peptides/proteins and allow mutations to modulate the toxicity of the peptides.³⁰

2.4. Molecular Modeling, Docking, and Molecular Dynamic Simulations of the Designed Multiepitope Vaccine with TLR-5. In order to predict the three-dimensional (3D) structures of the MEV and canine TLR-5, the I-Tasser program was used.^{31,32} The tertiary structures of the MEV and TLR-5 were further validated by generating Ramachandran plots using the ProCheck web server.

For docking the MEV to TLR-5, the HADDOCK server³³ was used. Further, all the MD simulations were performed with the GROMACS 2019 simulation program.³⁴ TLR-5 complexed with MEV was placed in a cubic box and solvated with TIP3P water molecules creating a solvent layer at least 12 Å thick. The Amber ff99SB-ILDN³⁵ force field was used to model the parameters of the proteins. Charge was neutralized by adding the appropriate number of K⁺ ions. The extra K⁺Cl⁻ ions were added to achieve a bulk ionic strength of 0.15 M using the Joung–Cheatham ion model.³⁶ The simulation box contains 453 556 water molecules, 1216 K⁺ ions, and 1229 Cl⁻ ions. The total number of atoms in the system was 1 377 736. The system was first minimized with 50 000 steps of the steepest descent method with 1000 kJ/mol nm² position restraint on protein heavy atoms. Further, minimization was carried out without any restraint on the protein. Equilibration of each system was carried out in a phased manner. First, a 100 ps NVT simulation was carried out with restraint on the heavy atoms of the protein. In the second step, a 100 ps NPT simulation with restraint on the heavy atoms of the protein was performed. Production simulations were run using the NPT ensemble for 100 ns. The temperature was maintained at 300 K using velocity rescaling with a coupling time of 0.1 ps. The pressure was maintained at 1 atm for NPT simulations using a

Parrinello–Rahman barostat³⁷ with a coupling time of 2 ps. Equations of motion were integrated using the leapfrog algorithm with a time step of 2.0 fs. The total electrostatic interactions were evaluated using the particle mesh Ewald (PME) summation.³⁸ Coulomb and van der Waals cutoffs of 1.0 nm were employed. Periodic boundary conditions in all directions were employed to mimic the bulk behavior. Bond lengths with hydrogen were constrained with the LINCS algorithm.³⁹ Coordinates were kept collecting in trajectory files every 10 ps. Trajectory processing and most of the analysis was performed using the GROMACS tools. The visualization and molecular graphics images were created using PYMOL⁴⁰ and VMD software.⁴¹ Graphs were plotted using in-house python scripts. In fact, our group has successfully employed a similar modeling and MD simulation protocol to study the structural stability of proteins^{42,43} and nucleic acid systems.^{44–51}

2.5. Immune Simulation. To determine the immunogenicity and immune response profile of the CanineCV MEV, the C-IMMSIM web server was used.⁵² The C-IMMSIM web server applies position-specific scoring matrices obtained from a machine learning approach to predict the immune response. It has been recommended that the minimum interval between the first and second dose of the vaccine should be weeks, and in some cases the minimum interval can be 8 weeks, 3 months, or 6 months.^{53,54} Hence, in this study the immune response of the vaccination was predicted using three injections at 4 week intervals.⁵⁵ In this analysis, the default parameters except the time step of injection were used. The time steps of 1, 84 (equivalent to 4 weeks), and 168 (equivalent to 8 weeks) were used.

2.6. Peptide Synthesis and Conjugation with Carrier Protein. One of the potential antigenic peptides with an RVRRHARASRSYRC sequence was custom-synthesized by GenScript (Piscataway, U.S.A.). The cysteine residue was added at the N-terminal position of the peptide and subsequently conjugated with keyhole limpet hemocyanin (KLH) to generate immunogen.

2.7. In Vivo Validation for Antibody Development and Assessment. KLH-conjugated peptide was inoculated in New Zealand rabbit. The affinity-purified antibody was retrieved by GenScript (Piscataway, U.S.A.). Since indirect enzyme-linked immunosorbent assay (ELISA) is usually employed to analyze the outcome of an immunological response, the antibody titer was therefore determined with indirect ELISA. Free peptide was used as the antigen at a coating concentration of 4 µg/mL and 100 µL/well for ELISA development. To minimize the background, cross-reactivity, and improve the lot-to-lot consistency, a unique GenScript mouse antirabbit IgG Fc antibody (cat. no. A01856) coupled to horseradish peroxidase (HRP) was used as the secondary antibody. The OD_{450nm} value was measured using an ELISA plate reader.

RESULTS AND DISCUSSION

3.1. Prediction of Antigenic Epitopes and Analysis of Their Antigenicity. The NetMHCIIpan 4.0 server was deployed for screening the epitopes from the capsid and replicase from three chosen strains of CanineCV. Our analyses resulted in the identification of 256 epitopes from the capsid protein and 289 epitopes from the replicase protein for each strain of CanineCV. On the basis of VaxiJen score (with a threshold value of ≥ 0.7), 100 epitopes were screened out from 256 epitopes of the capsid protein while 80 epitopes were

Table 1. Epitope Screening Based on the VaxiJen Score (≥ 0.7) from the NetMHCIIpan 4.0 Server

protein name	epitopes	protein ID	VaxiJen score	antigenicity
replicase	QVDQRGRDSRRGNP LGGRGHFEPARGDD	AVTS6110.1	1.5960	antigen
		AWN93250.1		
		ALG63389.1		
		QFU80922.1		
		AVTS6110.1	1.1867	antigen
		AWN93250.1		
		ALG63389.1		
		QFU80922.1		
		AVTS6111.1	1.0516	antigen
		AWN93251.1		
capsid	RVRRHARASRRSYR DPLQDRSSRSFNM	ALG63390.1		
		QBQ20241.1		
		AVTS6111.1	0.8144	antigen
		AWN93251.1		
		ALG63390.1		
		QBQ20241.1		
		AVTS6111.1	1.0997	antigen
		AWN93251.1		
		ALG63390.1		
		QBQ20241.1		

Table 2. List of the Antigenic Epitopes Based on the Genscript OptimumAntigen Tool and Analysis of Their Toxicity, Allergenicity, Interferon- γ Inducing Ability, and Conservancy^a

protein	peptide ^b	VaxiJen score	antigen/nonantigen	allergenicity	toxicity	interferon- γ inducing ability	conservancy
capsid	CDGEDQGRGNAQRSH	0.2792	nonantigen	nonallergen	nontoxin	negative	nonconserved
	CVPGRLLEPKDPNK	-0.1227	nonantigen	nonallergen	nontoxin	negative	nonconserved
	CQMKDMRPTTPDTST	0.7384	antigen	allergen	nontoxin	negative	conserved in only two strains
	APVKPTNDPQTETPC	0.6359	antigen	nonallergen	nontoxin	negative	conserved in only one strain
	CSGFKRGLTPKPMFT	0.1038	nonantigen	nonallergen	nontoxin	negative	conserved in all three strains
	CIAFKEFDYETGRQL	1.251	antigen	nonallergen	nontoxin	negative	conserved in all three strains
	CDPLQDRSSRSFNM	0.7415	antigen	nonallergen	nontoxin	negative	conserved in all three strains
	RVRRHARASRRSYRC	1.3046	antigen	nonallergen	nontoxin	negative	conserved in all three strains
	QVDQRGRDSRRGNPC	1.7055	antigen	nonallergen	nontoxin	negative	conserved in all three strains
	CESGEVSRQGKRNDL	0.9999	antigen	nonallergen	nontoxin	negative	conserved in only one strain
replicase	LGGRGHFEPARGDDC	0.9514	antigen	nonallergen	nontoxin	negative	conserved in all three strains
	CSPEMTTPRNWKTEV	-0.0674	nonantigen	allergen	nontoxin	negative	nonconserved
	CDRYPLRVETKGGT	0.8317	antigen	nonallergen	nontoxin	negative	conserved in only two strains
	CNRLPHEWYSDEIGN	0.019	nonantigen	nonallergen	nontoxin	positive	nonconserved
	PTPEEEAVKNLAPC	0.4023	antigen	nonallergen	nontoxin	negative	nonconserved
	CGCGKSRYCMETAPP	0.014	nonantigen	nonallergen	nontoxin	positive	nonconserved
	SNKDYCSKGGDILIC	0.4868	antigen	nonallergen	nontoxin	negative	conserved in only one strain
	ICGREVGENGTPHLC	-0.0113	nonantigen	nonallergen	nontoxin	negative	conserved in all three strains

^aThe selected epitopes are in bold and italic. ^bAn extra cysteine is added to the N- or C-terminus for the identified epitopes in order to facilitate conjugation while predicting the antigens using the OptimumAntigen design tool.

screened from 289 epitopes of the replicase protein for each strain. As a next step, we used the Genscript OptimumAntigen design tool, and we found eight antigenic epitopes from the capsid protein and 10 antigenic epitopes from the replicase protein of the CanineCV (Table S3). Finally, we chose those

epitopes that were commonly identified using two independent approaches: (a) NetMHCIIpan 4.0 and (b) Genscript OptimumAntigen design tool. The resulting five epitopes that were conserved among all the three chosen strains were used to generate the MEV construct (see Figure 1). For the

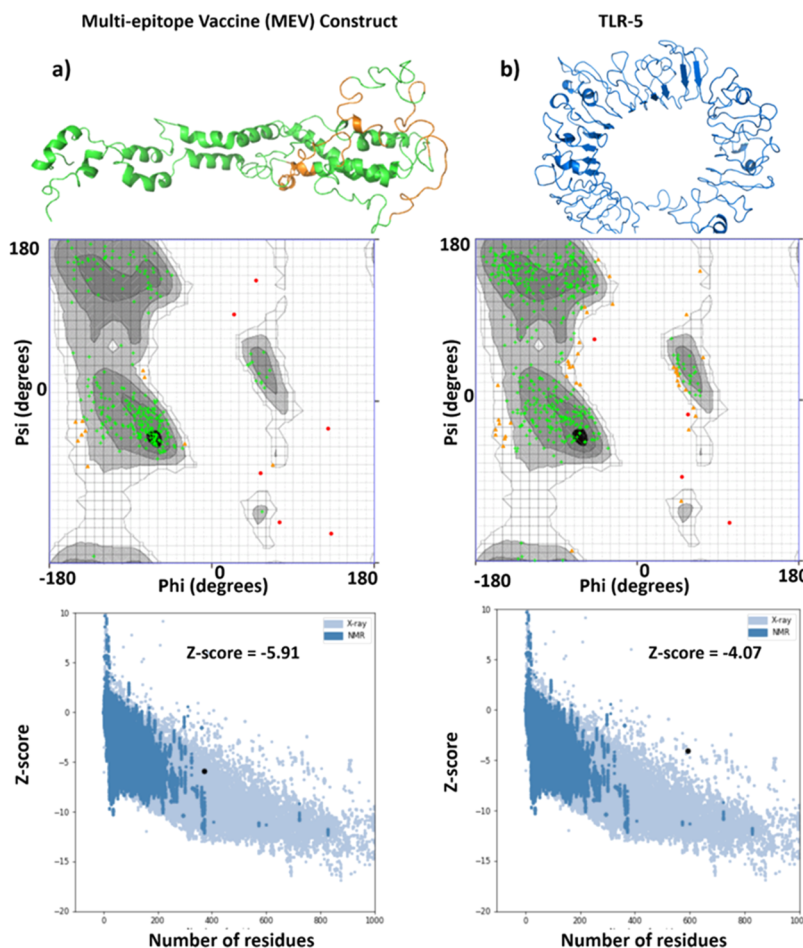


Figure 2. Cartoon representation of the modeled 3D structures of (a) the MEV construct, with the five epitopes in orange and the bacterial flagellin sequence at the N- and C-terminal position of the construct in green and (b) the Toll-like receptor 5(TLR-5) used in this study. Respective Ramachandran plots and Z-scores calculated by the Pro-SA web server are also shown with predicted structures. For the Ramachandran plot, black, light, and dark gray represent the core region (in green crosses), the white with black grid represents the allowed and generously allowed regions (in brown triangles), and the white and gray grid represents disallowed regions (in red circles).

replicase proteins, the epitopes QVDQRGRDSRRGNP and LGGRGHFEPARGDD were found to be conserved among all chosen strains. However, the epitopes RVRRHARASRRSYR, DPLQDRSSSRSFNM, and IAFKEFDYETGRQL were observed to be conserved for the capsid in all three CV strains considered in this study; see Table S3. Both the capsid and replicase proteins in all the chosen strains were also subjected to multiple sequence alignment (MSA) which revealed the identity to be greater than 94% between protein sequences (Tables S1 and S2). Since the Genscript OptimumAntigen and NetMHCIIpan 4.0 server both screen similar epitopes, based on the VaxiJen score, these epitopes can be considered antigenic and conserved, as provided in Table 1, Table 2, and Table S3. For the final MEV construct design, only those epitopes were selected which were predicted as being nontoxic, highly conserved, nonallergic, and antigenic by both VaxiJen and the Genscript OptimumAntigen tool.

3.2. CanineCV Vaccine Formulation and Determination of Its Physiochemical Properties. The designed MEV construct consisted of 372 amino acid residues. The vaccine included five immunogenic T cell epitopes, three adjuvants, RS09 having the sequence APPHALS, PADRE having sequence AKFVAATLKA, and an N-terminal and C-terminal sequence of *Salmonella typhimurium* flagellin protein

that were linked to the epitopes with the help of a GPGPG linker as an immune adjuvant to elicit a robust immune response.^{56,57} In fact, the flagellin's C-terminal D0 domain has been reported to be involved in TLR-5 activation.^{56,57} The sequence of the formulated MEV construct is shown in Figure 1. The selected five epitopes were CIAFKEFDYETGRQL, CDPLQDRSSSRSFNM, RVRRHARASRRSYRC, QVDQRGRDSRRGNPC, and LGGRGHFEPARGDDC which were predicted to be conserved in all the selected strains and were highly antigenic, nontoxic, and nonallergic, see Table S3.

The formulated vaccine was antigenic with an antigenic score of 0.5089 as calculated by the VaxiJen 2.0 server. The final vaccine had a molecular weight of 38.44 kDa and an isoelectric point (pI) of 9.91. The total numbers of negatively and positively charged amino acids were 27 and 39, respectively. The calculated aliphatic index (69.14) indicated a stable vaccine construct in a broad range of temperatures. Our vaccine had an estimated half-life of 30 h in mammalian reticulocytes (*in vitro*) and >20 h in *Saccharomyces cerevisiae* (*in vivo*) and >10 h in *Escherichia coli* (*in vivo*) as analyzed by the Expasy ProtParam server. Further, the predicted solubility of the vaccine was calculated to be 0.661 upon expression in *E. coli*. Finally, the physiochemical properties and antigenicity of the candidate CanineCV MEV construct were compared with

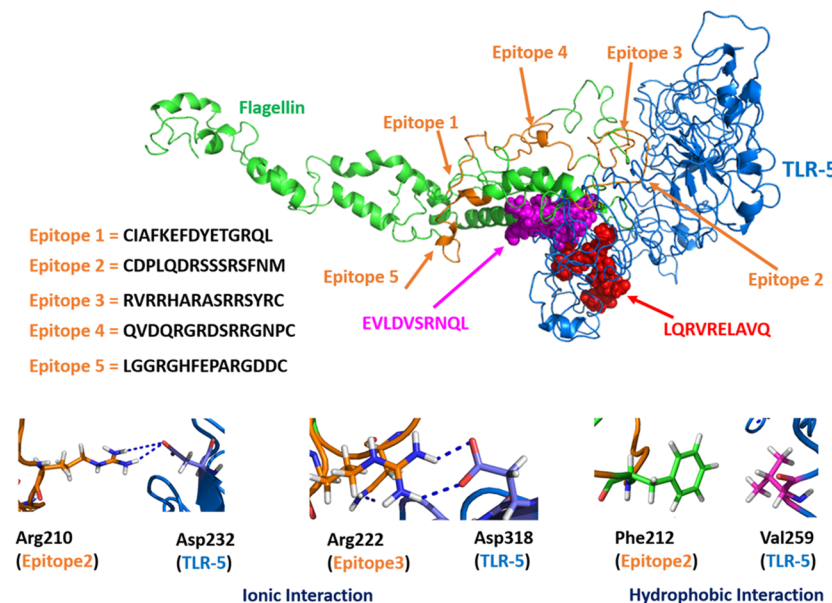


Figure 3. Top panel: docked complex of the MEV construct (green cartoon) and TLR-5 (marine blue cartoon). The hotspot residues used (see the Methods section for details) for information-driven docking are shown in spheres and colored in magenta and red for the MEV construct and the TLR-5 receptor, respectively. The epitope peptide sequences present in the MEV are also shown. Bottom panel: three representative interactions between amino acid residues of the immunogenic receptor (TLR-5) and epitopes 2 and 3 of the MEV construct.

other viral and cancer vaccine constructs designed using immunoinformatics approaches.^{55,58–60} The CanineCV MEV candidate has a very similar physiochemical property compared to the other vaccine constructs; see Table S4.

3.3. Modeling and Docking of TLR-5 and the Multiepitope Vaccine Construct. The tertiary structure of the final MEV construct and of the immunogenic TLR-5 was predicted using the I-TASSER program.⁶¹ In order to confirm the quality of the predicted structures, we calculated the Ramachandran plot of the modeled TLR-5 and vaccine construct along with the Z-scores from the ProSA web server.⁶² For the MEV construct, out of 372 residues, 76.6% of the residues were found to fall in the core-favored regions, 20.3% and 1.4% residues were in allowed and generously allowed regions, and the remaining 1.7% residues were observed under disallowed regions; see Figure 2a. For the TLR-5 receptor, 73% of the amino acids were found in the core acceptable region and the other 24.5% were observed under the allowed region, with an additional 1.5% falling under the generously allowed region and the remaining 1% in the disallowed regions of the Ramachandran plot; see Figure 2b. The Ramachandran plot calculated here is consistent with recent studies on different vaccine structures designed for different viruses.^{63,64}

Molecular docking of the modeled structure of the MEV construct with the modeled TLR-5 from *Canis lupus* was performed using the HADDOCK 2.4 web server in order to evaluate the interaction between the vaccine construct and TLR-5 which would probably elicit an immune response.⁴⁴ The data-driven docking of the designed multiepitope–TLR-5 complex was performed. The flagellin adjuvant, which is a bacterial protein, is known to specifically bind to TLR-5, which would probably elicit the innate immune response.⁵⁷ Here, we specifically used the information-driven docking where the information about which specific residues are involved in the interaction is needed to drive the docking calculations. Jacchieri et al. used a similar approach while using

complementary hydrophathy between the sequences of flagellin and TLR-5 to predict the potential binding sites and the structure of the complex.⁶⁵ The sequences “LQRVRELAVQ” and “EILDISRNQL” were predicted as the potential binding sites in flagellin and human TLR-5, respectively.⁴⁵ Since minor amino acid variations are observed for TLR-5 from *C. lupus*, the “EVLDVSRNQL” sequence was instead used here to drive the docking.

Docking of the vaccine construct to the TLR-5 receptor by HADDOCK resulted in 129 structures grouped in 11 clusters, which represent 64% of the water-refined HADDOCK-generated models. We had specifically chosen the top-ranked cluster with the lowest HADDOCK score. The HADDOCK score of -96.4 ± 5.1 indicated a good interaction between the vaccine construct and the TLR-5 receptor. The buried surface area (BSA) of the selected complex model was $1977.3 \pm 54.4 \text{ \AA}^2$. Figure 3 illustrates the molecular docking between the vaccine construct and the TLR-5 receptor. Our docking simulations predicted a structure where epitope 2 and epitope 3 are present in close proximity to the TLR-5 receptor. Two examples of salt bridges were present between Arg210 from epitope 2 and Asp232 from TLR-5 and between Arg222 from epitope 3 and Asp318 from TLR-5 (see Figure 3). Further, a hydrophobic interaction is present between Phe212 from epitope 2 and Val259 from TLR-5. In order to study the stability of the docked complex, it was subjected to MD simulations; see below for the detailed analysis.

3.4. Structural Stability of the MEV–TLR-5 Complex.

In order to study the structural stability of the docked complex of MEV and TLR-5, MD simulations were performed.⁶⁶ Three 100 ns long simulations of the complex were performed using GROMACS software,²⁶ with different initial velocities, which gave very similar results (Figure S1); therefore, only one will be discussed in the following. The root mean square deviation (RMSD) of the C α atoms from their initial position, which can be indicative of the stability or a possible conformational drift of the MEV–TLR-5 complex during the simulation time, was

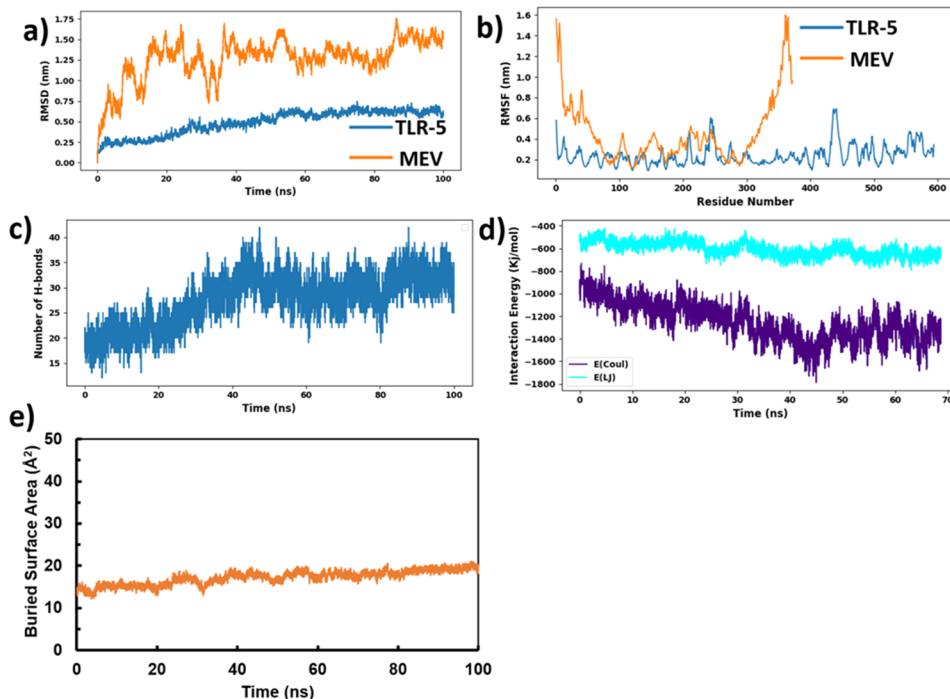


Figure 4. (a) Time evolution of the backbone RMSD of the TLR-5 and MEV constructs during MD simulations. (b) Backbone RMSF plots. (c) Time evolution of the number of hydrogen bonds between TLR-5 and the MEV. (d) Variation in the interaction energy plots with segregated electrostatics [E(Coul)] and van der Waals [E(LJ)] components. (e) Buried surface area of TLR-5 and the MEV construct.

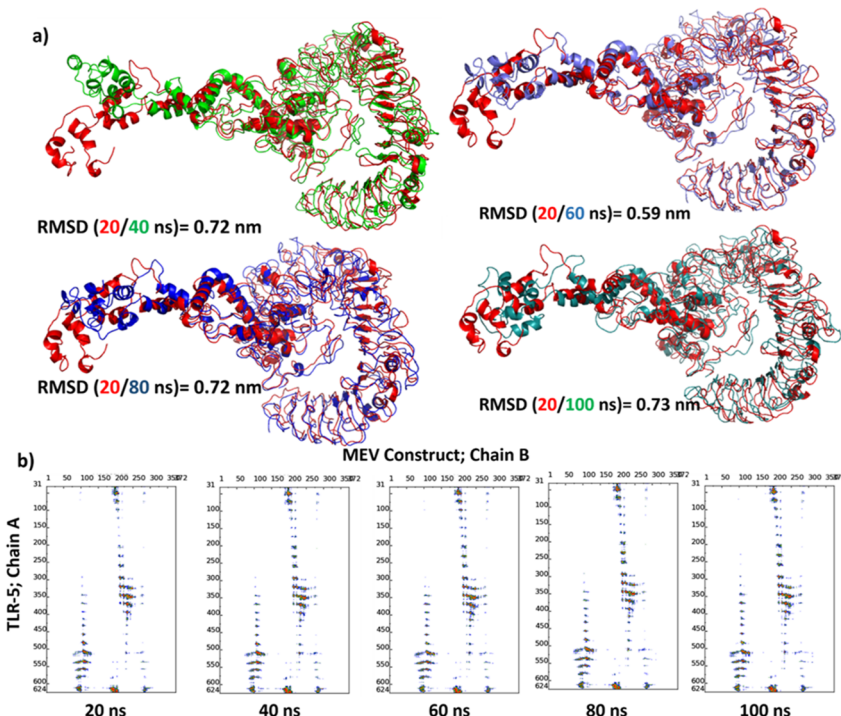


Figure 5. (a) Superimposition of selected snapshots (every 20 ns) of the TLR-5 and MEV constructs and their respective RMSD values. (b) Contact maps showing intermolecular contacts for the same snapshots. The dots at the crossover of two residues are colored in red, yellow, green, and blue if any pair of atoms is closer than 7, 10, 13, and 16 Å.

monitored and is plotted in Figure 4a. The calculated RMSD values of the docked TLR-5 and MEV complex after 40 and 100 ns simulations were 0.72 and 0.73 nm, respectively. The highest RMSD values were observed for the flexible terminal regions of the flagellin moiety of the MEV construct. In fact, the TLR-5 receptor alone was substantially stable (see Figure

4a), with an average RMSD value of 0.49 ± 0.15 nm. However, the predicted MEV possessed flexibility due to the presence of less structured epitope and linker regions, leading to the relatively high average RMSD value of 1.26 ± 0.25 nm. However, looking at Figure 4a, it is clear that the RMSD of the MEV got stabilized after 40 ns of simulation time. To get an

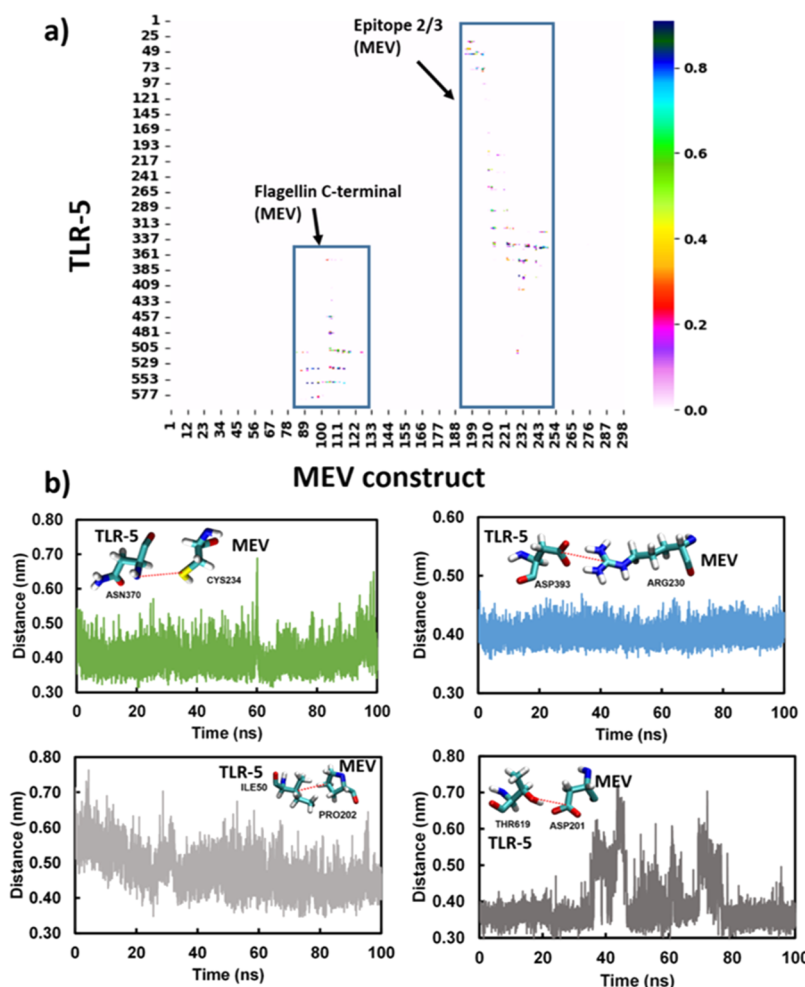


Figure 6. (a) MDcons consensus map of 1000 MD snapshots. The flagellin C-terminus and the region of epitopes 2 and 3 on the MEV that interact with TLR-5 are highlighted in blue boxes. The ICs with their rate of conservation are shown in distance plots. (b) Time evolution of four selected examples of conserved contacts (indicated by dark blue dots) between TLR-5 and the MEV.

understanding of the structure flexibility on a residue basis, we also plotted the root mean square fluctuation (RMSF) separately for the TLR-5 and the vaccine construct. Looking at Figure 4b, where the highly flexible regions are found associated with elevated fluctuations, it is evident that the $\text{C}\alpha$ atoms of entire TLR-5 structure have a limited flexibility. In contrast, a high fluctuation, with an average RMSF of 1.13 ± 0.6 nm, was observed for residues 1–90 and 312–372 of the MEV construct (regions associated with the N-terminal and C-terminal positions of flagellin). Furthermore, the number of intermolecular hydrogen bonds in the TLR-5–MEV construct remained constant after 20 ns of simulation (see Figure 4c). It is illustrated in Figure 4e that the buried surface area at the interface of the MEV and TLR-5 remained stable throughout the simulation time. Finally, we calculated the interaction energies between TLR-5 and the MEV and decomposed it into its Coulombic component [$E(\text{Coul})$], which represents the electrostatics interaction, and the Lennard-Jones [$E(\text{LJ})$] potential component that accounts for the van der Waals interactions. Considering that the complex remained stable after 30 ns of simulation time, the interaction energy components were plotted for the final 70 ns. From Figure 4d, it is evident that the predominant interaction that stabilized the overall TLR-5 and MEV complex stemmed from the electrostatic component of the interaction, with the average

electrostatics energy being -1250.57 ± 167.7 kcal/mol. In contrast, the average $E(\text{LJ})$ contribution was found to be -608.68 ± 63.5 kcal/mol. Thus, our overall energetic analysis clearly depicted that the stabilization of the interaction between TLR-5 and the MEV is predominantly contributed by the electrostatic component of the interaction energy.

3.5. Detailed Analysis of Snapshots Obtained during the MD Simulations and Their Comparison with the Initial Model of the TLR-5–MEV Construct. We carried out a detailed analysis of the noncovalent interactions occurring between the MEV and TLR-5 using an in-house script. The docked TLR-5 and MEV construct complex was stabilized by a network of 60 intermolecular H-bonding interactions within 3.5 Å, 13 hydrophobic interactions, and 11 salt-bridge interactions within 5 and 6 Å distance cutoffs, respectively. The list of noncovalent interactions is reported in Table S5. Out of the total 11 salt bridges, two existed between epitope 2 of the vaccine construct and TLR-5 and three existed between epitope 3 of the vaccine construct and TLR-5. The distance plots for the $\text{C}\alpha$ atoms of residues involved in the salt bridges indicated the stability of these interactions throughout the simulation time. This further reinforced the stability of the predicted vaccine construct and the TLR-5 immune receptor. To further assess the stability of the overall complex, the superimposition of structures at different time steps was done,

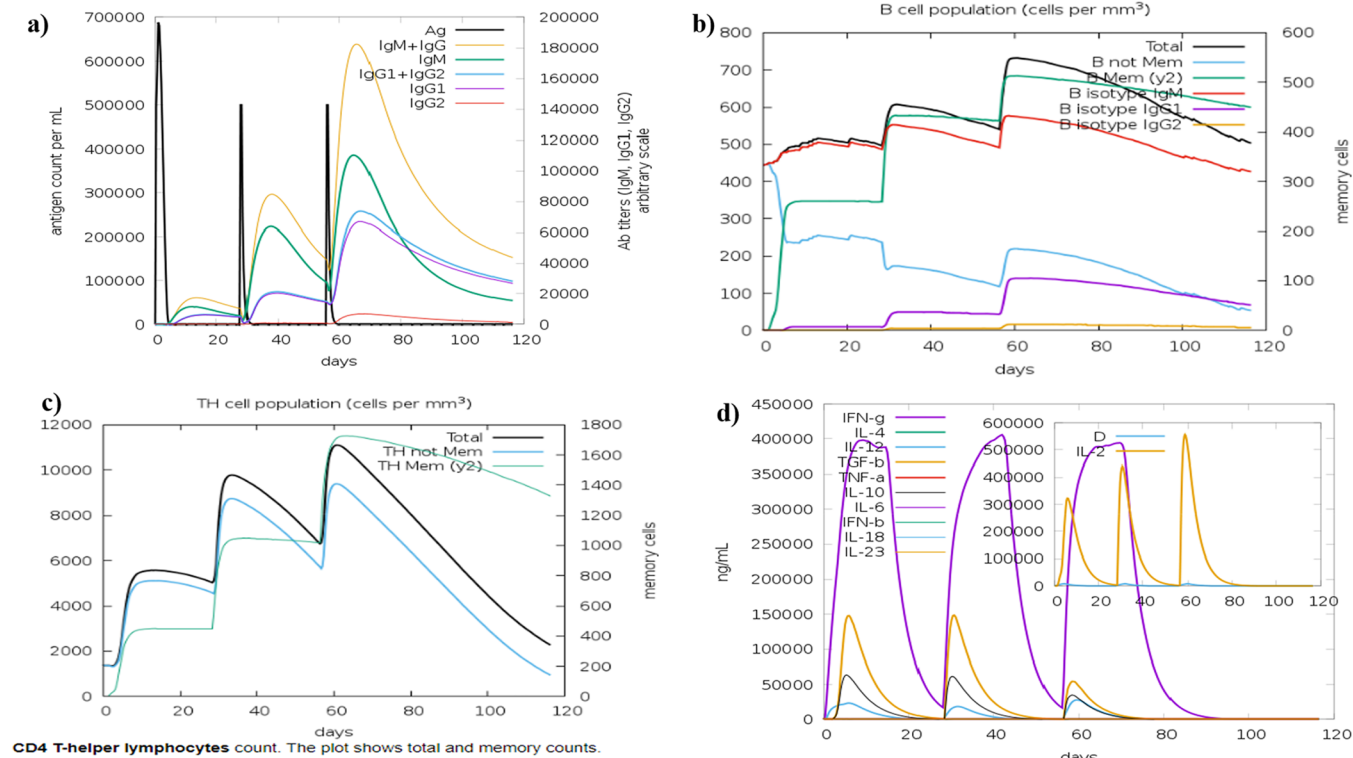


Figure 7. C-IMMSIM analysis used to predict the immune response after the vaccine construct administration: (a) antigen count and antibody titer with specific subclasses; (b) B-cell population; (c) T-helper cell population; (d) concentration of cytokines and interleukins.

which resulted in good overlap between the structures. From Figure 5a, it is clear that the complex remained stable with a low RMSD for the selected snapshots. Furthermore, an interface analysis for selected snapshots was performed between TLR-5 and the docked vaccine construct using the COCOMAPS tool^{67,68} (see Figure 5b). Contact maps, specifically “distance range maps” were computed, where the dots at the crossover of two residues belonging, respectively, to the vaccine construct and TLR-5 are colored in red, yellow, green, and blue if any pair of their atoms is closer than 7, 10, 13, and 16 Å. Looking at Figure 5b, it is evident that the interface remained stable, in terms of inter-residue contacts, for the selected snapshots, notwithstanding the observed flexibility in the peripheral regions of the MEV construct. Using a cutoff distance of 5 Å between two atoms to define a contact, 73 contacts are observed between hydrophilic residues, 71 between a hydrophilic and hydrophobic residue, and 39 between two hydrophobic residues.

To further assess the stability of the MEV construct–TLR-5 complex, the conservation of inter-residue contacts (ICs) at the interface along the simulation time was plotted using the MDcons program.⁶⁹ The conservation under dynamic conditions of ICs between macromolecules giving a stable complex is an efficient measure of the similarity between different snapshots, focused on the region of interest that is the biological interface. The consensus map of 1000 MD snapshots is plotted in Figure 6a, and distances along the simulation time for selected conserved ICs are plotted in Figure 6b. The overall conservation of the ICs at the interface during the MD simulations could be visually appreciated by looking at the MD consensus map of Figure 6a. From the MD consensus plot, it was clear that many contacts between the MEV construct and TLR-5 remained stable throughout the simulation time.

MDcons analysis resulted in a C_{70} value of 0.64, which means that 64% of the ICs were conserved in at least 70% of the frames. Thus, a pretty high conservation of the interface during the simulation time is observed. A few examples among the ICs that remained stable over the simulation time, specifically between TLR-5 and epitope 2 and epitope 3 of the MEV, are illustrated in Figure 6b. In particular, a salt-bridge interaction existed between Asp393 of TLR-5 and Arg230 from epitope 3 of the MEV construct that remained stable along the simulation time with an average Asp393-(CB)–Arg230(CZ) distance of 0.40 ± 0.02 nm, a hydrogen-bonding interaction between Thr619 of TLR-5 and Asp201 from epitope 2 of the MEV was observed that remained stable with an average Thr619(CB)–Asp201(CG) distance of 0.47 ± 0.06 nm, and a hydrophobic contact between Ile50 from TLR-5 and Pro202 from epitope 2 of the MEV construct with an average Ile50(CB)–Pro202(CB) distance of 0.39 ± 0.06 nm was also observed to be stable along the simulation time.

3.6. Immune Response Profile Using *In Silico* Immune Simulation. The immune simulation shows that first injection of the vaccine increased the levels of immunoglobulin activity, in particular for the IgG1 + IgG2, IgM, and IgG + IgM antibodies. Moreover, the second and third injections significantly increased the antibody titer in comparison to the first injection; see Figure 7a. The third injection also increased the titer of the IgG2 antibody. This analysis also predicted that the immunization could stimulate the total B-cell population after every injection of the vaccine candidate; see Figure 7b. Further, an increase in IgM was also observed, an antibody that is generated after the initial exposure to antigen. Additionally, the expression of memory cells is also increased after each vaccination suggesting activation of a robust secondary immune response. The overall population of

T-helper cells also gets increased after each vaccination; see Figure 7c. Interestingly, the vaccination stimulated interferon- γ , TGF- β , interleukin-10, and interleukin-12 production; see Figure 7d. However, the interferon- γ population after each immunization was almost the same and the population of TGF- β , interleukin-10, and interleukin-12 decreased after the third vaccination (Figure 4). Overall, the C-IMMSIM simulations predicted that the CanineCV MEV could activate the immune response.

3.7. Peptide Synthesis and Conjugation to Carrier Protein.

The selected capsid protein epitope RVRRHARASRRSYRC was custom-synthesized by GenScript (Piscataway, U.S.A.). The cysteine residue was added to the N-terminal position of the immunogenic peptide. The peptide antigen containing cysteine is indicated as CRVRRHARASRRSYRC which was subsequently conjugated with KLH.

3.8. In Vivo Validation for Antibody Development and Assessment.

The affinity-purified concentration of the antibody was found to be 287 $\mu\text{g}/\text{mL}$ of the antiserum of New Zealand white rabbit subcutaneously immunized with the KLH-conjugated peptide. In order to confirm whether the KLH conjugate peptide could stimulate humoral immunity and produce antibodies, indirect ELISA was performed, and a positive correlation was found between the serum antibody and ELISA OD values (Figure 8a). Further, the antibody titer was also determined. The antibody titer is expressed as the inverse of the highest dilution of the antibody which gives a positive result in ELISA. The serum collected from the rabbit was serially diluted more than 8-fold. Interestingly, 2–6-fold diluted aliquots (i.e., 1:1000 to 1:64 000) showed a positive

result on ELISA, as indicated by the titer value of ≥ 2.28 with a reference signal/blank of ≥ 2.1 (see the Supporting Information for more details). However, no color was observed when IgG in the range of 1:1000 to 1:512 000 was incubated with the antigen; see Figure 8b. These results clearly indicate that the vaccine designed in this study is a promising immunogen which could effectively stimulate the production of antibodies *in vivo*.

A multiepitope peptide vaccine targeting multiple antigens approach has been extensively explored for vaccine development for animal, fish, and poultry viral diseases including avian avula virus, foot and mouth disease virus, and seven banded grouper nervous necrosis virus.^{70–72} However, no vaccine candidate has been reported for CanineCV until now. Multiepitopes-based vaccine-based prediction for CanineCV could assist in managing severe problems of gastroenteritis and diarrhea in dog populations. Further, it could be effectively successful in terms of saving time without conducting multiple random hit and trial approaches. Deploying this strategy, we have recently screened the proteins of CanineCV in order to predict the epitopes using the latest neural network algorithm dependent tools like the NetMHC server, along with antigenicity and toxicity analyses criteria, in order to brief the major group of considerable epitopes during subsequent steps of screening.²² In the present study, we extended this robust immunoinformatics approach to identify a novel CD4 $^+$ T cell epitope-based MEV candidate for CanineCV while taking into account different strains of the *C. lupus* family isolated on different continents. Interestingly, three epitopes identified were found to be conserved in all the strains considered in the present work, and one of the potential epitopes was further synthesized for *in vivo* analysis. As a first step, we predicted 545 MHCII binding CD4 $^+$ T cell epitope peptides for each strain. Further, we refined five conserved epitopes among all the three strains of CanineCV according to their antigenicity score. The antigenic and nontoxic epitopes “CIAFKEFDYETGRQL”, “CDPLQDRSSSRSFNM”, “RVR-RHARASRRSYRC”, “QVDQRGRDSSRRGNPC”, and “LGG-RGHFEPARGDDC” that were conserved among all the three CanineCV strains were selected for final vaccine construct. Once the epitopes were identified, they were linked by GPGPG linkers to adjuvants such as RS09 and flagellin protein along with the PADRE sequence to craft the final vaccine construct. Subsequently, TLR-5 was selected as the receptor for MEV since TLR has been reported for its role in the internalization of a vaccine construct which would probably elicit an immune response.⁷³ Moreover, TLR-5 has been recently used for the successful internalization of the vaccine constructs for viral diseases including West Nile virus, HBV, influenza virus, and porcine circovirus.⁷⁴ Overall, our computational analyses suggest that the novel MEV construct identified is not only a potent immunogen but also nontoxic and nonallergenic in nature. Further, the *in vivo* analysis of MEV ensured CD4 $^+$ T-cell-dependent generation of antibodies, thus clearly indicating vaccine potential to induce the immune response.

CONCLUSION

No MEV-based vaccine has been reported for CanineCV to date. In the present study, a successful attempt is made to design a CD4 $^+$ T-cell-based MEV against CanineCV. Immunoinformatics and *in silico* approaches are used to design a highly antigenic and immunogenic vaccine candidate which is

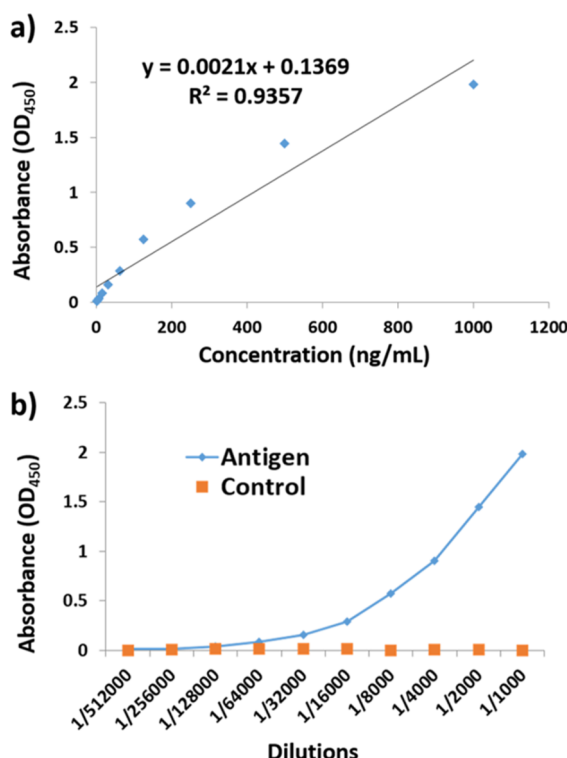


Figure 8. (a) Plot showing the linear correlation between the absorbance (OD_{450}) values and concentration of serum antibody (ng/mL). (b) ELISA assay plot of OD_{450} values and serum dilutions from 1:1000 to 1:512 000 of CanineCV antibody and IgG control. The OD_{450} values can be inversely correlated to the serum dilutions.

found to be safe, stable, and strongly interacting with canine TLR-5. Furthermore, the *in vivo* generation of the antibodies in response to the selected epitope corroborates that the designed vaccine construct appears to be a promising candidate for a vaccine against CanineCV.

■ ASSOCIATED CONTENT

§ Supporting Information

The Supporting Information is available free of charge at <https://pubs.acs.org/doi/10.1021/acspptsci.2c00130>.

RMSD of trial simulations, multiple sequence alignments of replicase and capsid proteins, epitope conservancy analysis, filtered epitopes, Genscript antigen design results, and antibody purification results ([PDF](#))

■ AUTHOR INFORMATION

Corresponding Authors

Abdul Rajjak Shaikh — Department of Research and Innovation, STEMskills Research and Education Lab Private Limited, Faridabad 121002 Haryana, India; orcid.org/0000-0003-4444-0684; Email: razzaqsk@gmail.com

Luigi Cavallo — Physical Sciences and Engineering Division, Kaust Catalysis Center, King Abdullah University of Science and Technology, Thuwal 23955-6900, Saudi Arabia; orcid.org/0000-0002-1398-338X; Email: luigi.cavallo@kaust.edu.sa

Mohit Chawla — Physical Sciences and Engineering Division, Kaust Catalysis Center, King Abdullah University of Science and Technology, Thuwal 23955-6900, Saudi Arabia; orcid.org/0000-0002-3332-3055; Email: mohit.chawla@kaust.edu.sa, Mohitchawla.bt@gmail.com

Authors

Vikas Kaushik — Domain of Bioinformatics, School of Bio-Engineering and Bio-Sciences, Lovely Professional University, Phagwara 144001 Punjab, India

Pankaj Jain — Domain of Bioinformatics, School of Bio-Engineering and Bio-Sciences, Lovely Professional University, Phagwara 144001 Punjab, India

Nahid Akhtar — Domain of Bioinformatics, School of Bio-Engineering and Bio-Sciences, Lovely Professional University, Phagwara 144001 Punjab, India

Amit Joshi — Domain of Bioinformatics, School of Bio-Engineering and Bio-Sciences, Lovely Professional University, Phagwara 144001 Punjab, India

Lovi Raj Gupta — Domain of Bioinformatics, School of Bio-Engineering and Bio-Sciences, Lovely Professional University, Phagwara 144001 Punjab, India

Ravneet Kaur Grewal — Department of Research and Innovation, STEMskills Research and Education Lab Private Limited, Faridabad 121002 Haryana, India

Romina Oliva — Department of Sciences and Technologies, University Parthenope of Naples, I-80143 Naples, Italy

Complete contact information is available at:

<https://pubs.acs.org/10.1021/acspptsci.2c00130>

Notes

The authors declare the following competing financial interest(s): Authors R.K.G. and A.R.S. were employed by the company STEMskills Research and Education Lab Private Limited, Faridabad, Haryana, India. The remaining authors

declare that the research was conducted in the absence of any commercial or financial relationships that could be construed as a potential conflict of interest.

■ ACKNOWLEDGMENTS

The research reported in this publication was supported by funding from King Abdullah University of Science and Technology (KAUST). For computer time, this research used the resources of the Supercomputing Laboratory at King Abdullah University of Science and Technology (KAUST) in Thuwal, Saudi Arabia. The authors would also like to acknowledge team members from STEMskills Research and Education Lab Private Limited for critical reading of the manuscript and computational support.

■ REFERENCES

- (1) Kapoor, A.; Dubovi, E. J.; Henriquez-Rivera, J. A.; Lipkin, W. I. Complete genome sequence of the first canine circovirus. *J. Virol* **2012**, *86* (12), 7018.
- (2) Kotsias, F.; Bucafusco, D.; Nunez, D. A.; Lago Borisovsky, L. A.; Rodriguez, M.; Bratanich, A. C. Genomic characterization of canine circovirus associated with fatal disease in dogs in South America. *PLoS One* **2019**, *14* (6), e0218735.
- (3) Giraldo-Ramirez, S.; Rendon-Marin, S.; Vargas-Bermudez, D. S.; Jaime, J.; Ruiz-Saenz, J. First detection and full genomic analysis of Canine Circovirus in CPV-2 infected dogs in Colombia, South America. *Sci. Rep* **2020**, *10* (1), 17579.
- (4) Weber, M. N.; Cibulski, S. P.; Olegario, J. C.; da Silva, M. S.; Puhl, D. E.; Mosena, A. C. S.; Alves, C.; Paim, W. P.; Baumbach, L. F.; Mayer, F. Q.; Fernandes, A. R. F.; Azevedo, S. S.; Canal, C. W. Characterization of dog serum virome from Northeastern Brazil. *Virology* **2018**, *525*, 192–199.
- (5) Dowgier, G.; Lorusso, E.; Decaro, N.; Desario, C.; Mari, V.; Lucente, M. S.; Lanave, G.; Buonavoglia, C.; Elia, G. A molecular survey for selected viral enteropathogens revealed a limited role of Canine circovirus in the development of canine acute gastroenteritis. *Vet. Microbiol.* **2017**, *204*, 54–58.
- (6) Tuong, N. M.; Piewbang, C.; Rungsipipat, A.; Techangamsuwan, S. Detection and molecular characterization of two canine circovirus genotypes co-circulating in Vietnam. *Vet Q* **2021**, *41* (1), 232–241.
- (7) Turan, T.; Isidan, H. Molecular characterization of canine astrovirus, vesivirus and circovirus, isolated from diarrheic dogs in Turkey. *Iran J. Vet. Res.* **2020**, *21* (3), 172–179.
- (8) Piewbang, C.; Jo, W. K.; Puff, C.; van der Vries, E.; Kesdangsakonwut, S.; Rungsipipat, A.; Krappa, J.; Jung, K.; Baumgartner, W.; Techangamsuwan, S.; Ludlow, M.; Osterhaus, A. Novel canine circovirus strains from Thailand: Evidence for genetic recombination. *Sci. Rep* **2018**, *8* (1), 7524.
- (9) Sun, W.; Zhang, H.; Zheng, M.; Cao, H.; Lu, H.; Zhao, G.; Xie, C.; Cao, L.; Wei, X.; Bi, J.; Yi, C.; Yin, G.; Jin, N. The detection of canine circovirus in Guangxi. *China. Virus Res.* **2019**, *259*, 85–89.
- (10) Li, L.; McGraw, S.; Zhu, K.; Leutenegger, C. M.; Marks, S. L.; Kubiski, S.; Gaffney, P.; Dela Cruz, F. N., Jr.; Wang, C.; Delwart, E.; Pesavento, P. A. Circovirus in tissues of dogs with vasculitis and hemorrhage. *Emerg Infect Dis* **2013**, *19* (4), 534–541.
- (11) Thaiwong, T.; Wise, A. G.; Maes, R. K.; Mullaney, T.; Kiupel, M. Canine Circovirus 1 (CaCV-1) and Canine Parvovirus 2 (CPV-2): Recurrent Dual Infections in a Papillon Breeding Colony. *Vet Pathol* **2016**, *53* (6), 1204–1209.
- (12) Balboni, A.; Terrusi, A.; Urbani, L.; Troia, R.; Stefanelli, S. A. M.; Giunti, M.; Battilani, M. Canine circovirus and Canine adenovirus type 1 and 2 in dogs with parvoviral enteritis. *Vet Res. Commun.* **2022**, *46* (1), 223–232.
- (13) Zaccaria, G.; Malatesta, D.; Scipioni, G.; Di Felice, E.; Campolo, M.; Casaccia, C.; Savini, G.; Di Sabatino, D.; Lorusso, A. Circovirus in domestic and wild carnivores: An important opportunistic agent? *Virology* **2016**, *490*, 69–74.

- (14) Urbani, L.; Tryland, M.; Ehrlich, D.; Fuglei, E.; Battilani, M.; Balboni, A. Ancient origin and genetic segregation of canine circovirus infecting arctic foxes (*Vulpes lagopus*) in Svalbard and red foxes (*Vulpes vulpes*) in Northern Norway. *Transbound Emerg Dis* **2021**, *68* (3), 1283–1293.
- (15) Franzo, G.; Menandro, M. L.; Tucciarone, C. M.; Barbierato, G.; Crovato, L.; Mondin, A.; Libanora, M.; Obber, F.; Orusa, R.; Robertto, S.; Citterio, C.; Grassi, L. Canine Circovirus in Foxes from Northern Italy: Where Did It All Begin? *Pathogens* **2021**, *10* (8), 1002.
- (16) Bhardwaj, A.; Sharma, R.; Grover, A. Immuno-informatics guided designing of a multi-epitope vaccine against Dengue and Zika. *J. Biomol Struct Dyn* **2021**, *1*–15.
- (17) Dixit, N. K. Design of Monovalent and Chimeric Tetravalent Dengue Vaccine Using an Immunoinformatics Approach. *Int. J. Pept Res. Ther* **2021**, *27* (4), 2607–2624.
- (18) Ali, M.; Pandey, R. K.; Khatoon, N.; Narula, A.; Mishra, A.; Prajapati, V. K. Exploring dengue genome to construct a multi-epitope based subunit vaccine by utilizing immunoinformatics approach to battle against dengue infection. *Sci. Rep* **2017**, *7* (1), 9232.
- (19) Cuspoca, A. F.; Diaz, L. L.; Acosta, A. F.; Penalosa, M. K.; Mendez, Y. R.; Clavijo, D. C.; Yosa Reyes, J. An Immunoinformatics Approach for SARS-CoV-2 in Latam Populations and Multi-Epitope Vaccine Candidate Directed towards the World's Population. *Vaccines-Basel* **2021**, *9* (6), 581.
- (20) Krishnan, G. S.; Joshi, A.; Akhtar, N.; Kaushik, V. Immunoinformatics designed T cell multi epitope dengue peptide vaccine derived from non structural proteome. *Microb. Pathog.* **2021**, *150*, 104728.
- (21) Kaushik, V.; G, S. K.; Gupta, L. R.; Kalra, U.; Shaikh, A. R.; Cavallo, L.; Chawla, M. Immunoinformatics Aided Design and In-Vivo Validation of a Cross-Reactive Peptide Based Multi-Epitope Vaccine Targeting Multiple Serotypes of Dengue Virus. *Front Immunol* **2022**, *13*, 865180.
- (22) Jain, P.; Joshi, A.; Akhtar, N.; Krishnan, S.; Kaushik, V. An immunoinformatics study: designing multivalent T-cell epitope vaccine against canine circovirus. *J. Genet Eng. Biotechnol* **2021**, *19* (1), 121.
- (23) Swain, S. L.; McKinstry, K. K.; Strutt, T. M. Expanding roles for CD4(+) T cells in immunity to viruses. *Nat. Rev. Immunol* **2012**, *12* (2), 136–48.
- (24) Reynisson, B.; Alvarez, B.; Paul, S.; Peters, B.; Nielsen, M. NetMHCpan-4.1 and NetMHCIIpan-4.0: improved predictions of MHC antigen presentation by concurrent motif deconvolution and integration of MS MHC eluted ligand data. *Nucleic Acids Res.* **2020**, *48* (W1), W449–W454.
- (25) Reynisson, B.; Barra, C.; Kaabinejadian, S.; Hildebrand, W. H.; Peters, B.; Nielsen, M. Improved Prediction of MHC II Antigen Presentation through Integration and Motif Deconvolution of Mass Spectrometry MHC Eluted Ligand Data. *J. Proteome Res.* **2020**, *19* (6), 2304–2315.
- (26) Dhandha, S. K.; Vir, P.; Raghava, G. P. Designing of interferon-gamma inducing MHC class-II binders. *Biol. Direct* **2013**, *8*, 30.
- (27) Gasteiger, E.; Hoogland, C.; Gattiker, A.; Duvaud, S.; Wilkins, M.; Appel, R.; Bairoch, A. *The Proteomics Protocols Handbook*; Humana Press Inc.: Totowa, NJ, 2005.
- (28) Doytchinova, I. A.; Flower, D. R. VaxiJen: a server for prediction of protective antigens, tumour antigens and subunit vaccines. *BMC Bioinformatics* **2007**, *8*, 4.
- (29) Doytchinova, I. A.; Flower, D. R. Identifying candidate subunit vaccines using an alignment-independent method based on principal amino acid properties. *Vaccine* **2007**, *25* (5), 856–866.
- (30) Gupta, S.; Kapoor, P.; Chaudhary, K.; Gautam, A.; Kumar, R.; Open Source Drug Discovery, Consortium; Raghava, G. P. In silico approach for predicting toxicity of peptides and proteins. *PLoS One* **2013**, *8* (9), e73957.
- (31) David, A.; Islam, S.; Tankhilevich, E.; Sternberg, M. J. E. The AlphaFold Database of Protein Structures: A Biologist's Guide. *J. Mol. Biol.* **2022**, *434* (2), 167336.
- (32) Jumper, J.; Evans, R.; Pritzel, A.; Green, T.; Figurnov, M.; Ronneberger, O.; Tunyasuvunakool, K.; Bates, R.; Zidek, A.; Potapenko, A.; et al. Highly accurate protein structure prediction with AlphaFold. *Nature* **2021**, *596* (7873), 583.
- (33) van Zundert, G. C. P.; Rodrigues, J.; Trellet, M.; Schmitz, C.; Kastritis, P. L.; Karaca, E.; Melquiond, A. S. J.; van Dijk, M.; de Vries, S. J.; Bonvin, A. The HADDOCK2.2 Web Server: User-Friendly Integrative Modeling of Biomolecular Complexes. *J. Mol. Biol.* **2016**, *428* (4), 720–725.
- (34) Abraham, M. J.; Murtola, T.; Schulz, R.; Päll, S.; Smith, J. C.; Hess, B.; Lindahl, E. GROMACS: High performance molecular simulations through multi-level parallelism from laptops to supercomputers. *SoftwareX* **2015**, *1*–2, 19–25.
- (35) Lindorff-Larsen, K.; Piana, S.; Palmo, K.; Maragakis, P.; Klepeis, J. L.; Dror, R. O.; Shaw, D. E. Improved side-chain torsion potentials for the Amber ff99SB protein force field. *Proteins* **2010**, *78* (8), 1950–8.
- (36) Joung, I. S.; Cheatham, T. E. Determination of alkali and halide monovalent ion parameters for use in explicitly solvated biomolecular simulations. *J. Phys. Chem. B* **2008**, *112* (30), 9020–9041.
- (37) Parrinello, M.; Rahman, A. Polymorphic Transitions in Single-Crystals - a New Molecular-Dynamics Method. *J. Appl. Phys.* **1981**, *52* (12), 7182–7190.
- (38) Darden, T.; York, D.; Pedersen, L. Particle Mesh Ewald - an N.Log(N) Method for Ewald Sums in Large Systems. *J. Chem. Phys.* **1993**, *98* (12), 10089–10092.
- (39) Hess, B.; Bekker, H.; Berendsen, H. J. C.; Fraaije, J. G. E. M. LINCS: A linear constraint solver for molecular simulations. *J. Comput. Chem.* **1997**, *18* (12), 1463–1472.
- (40) Humphrey, W.; Dalke, A.; Schulten, K. VMD: Visual molecular dynamics. *J. Mol. Graph Model* **1996**, *14* (1), 33–38.
- (41) Humphrey, W.; Dalke, A.; Schulten, K. VMD: visual molecular dynamics. *J. Mol. Graphics* **1996**, *14* (1), 33.
- (42) Oliva, R.; Shaikh, A. R.; Petta, A.; Vangone, A.; Cavallo, L. D936Y and Other Mutations in the Fusion Core of the SARS-CoV-2 Spike Protein Heptad Repeat 1: Frequency, Geographical Distribution, and Structural Effect. *Molecules* **2021**, *26* (9), 2622.
- (43) Grewal, R. K.; Shaikh, A. R.; Gorle, S.; Kaur, M.; Videira, P. A.; Cavallo, L.; Chawla, M. Structural Insights in Mammalian Sialyltransferases and Fucosyltransferases: We Have Come a Long Way, but It Is Still a Long Way Down. *Molecules* **2021**, *26* (17), 5203.
- (44) Chawla, M.; Credendino, R.; Poater, A.; Oliva, R.; Cavallo, L. Structural stability, acidity, and halide selectivity of the fluoride riboswitch recognition site. *J. Am. Chem. Soc.* **2015**, *137* (1), 299–306.
- (45) Chawla, M.; Gorle, S.; Shaikh, A. R.; Oliva, R.; Cavallo, L. Replacing thymine with a strongly pairing fifth base: A combined quantum mechanics and molecular dynamics study. *Comput. Struct Biotechnol J.* **2021**, *19*, 1312–1324.
- (46) Kalra, K.; Gorle, S.; Cavallo, L.; Oliva, R.; Chawla, M. Occurrence and stability of lone pair-pi and OH-pi interactions between water and nucleobases in functional RNAs. *Nucleic Acids Res.* **2020**, *48* (11), 5825–5838.
- (47) Flamme, M.; Rothlisberger, P.; Levi-Acobas, F.; Chawla, M.; Oliva, R.; Cavallo, L.; Gasser, G.; Marliere, P.; Herdewijn, P.; Hollenstein, M. Enzymatic Formation of an Artificial Base Pair Using a Modified Purine Nucleoside Triphosphate. *ACS Chem. Biol.* **2020**, *15* (11), 2872–2884.
- (48) Chawla, M.; Poater, A.; Besalu-Sala, P.; Kalra, K.; Oliva, R.; Cavallo, L. Theoretical characterization of sulfur-to-selenium substitution in an emissive RNA alphabet: impact on H-bonding potential and photophysical properties. *Phys. Chem. Chem. Phys.* **2018**, *20* (11), 7676–7685.
- (49) Chawla, M.; Credendino, R.; Oliva, R.; Cavallo, L. Structural and Energetic Impact of Non-Natural 7-Deaza-8-Azaadenine and Its 7-Substituted Derivatives on H-Bonding Potential with Uracil in RNA Molecules. *J. Phys. Chem. B* **2015**, *119* (41), 12982–9.
- (50) Chawla, M.; Oliva, R.; Bujnicki, J. M.; Cavallo, L. An atlas of RNA base pairs involving modified nucleobases with optimal

- geometries and accurate energies. *Nucleic Acids Res.* **2015**, *43* (14), 6714–29.
- (51) Chawla, M.; Abdel-Azeim, S.; Oliva, R.; Cavallo, L. Higher order structural effects stabilizing the reverse Watson-Crick Guanine-Cytosine base pair in functional RNAs. *Nucleic Acids Res.* **2014**, *42* (2), 714–26.
- (52) Rapin, N.; Lund, O.; Bernaschi, M.; Castiglione, F. Computational Immunology Meets Bioinformatics: The Use of Prediction Tools for Molecular Binding in the Simulation of the Immune System. *PLoS One* **2010**, *5* (4), e9862.
- (53) Robinson, C. L.; Romero, J. R.; Kempe, A.; Pellegrini, C. Advisory Committee on Immunization Practices Recommended Immunization Schedule for Children and Adolescents Aged 18 Years or Younger - United States, 2017. *MMWR Morb. Mortal. Wkly. Rep.* **2017**, *66* (5), 134–135.
- (54) Castiglione, F.; Mantile, F.; De Berardinis, P.; Prisco, A. How the Interval between Prime and Boost Injection Affects the Immune Response in a Computational Model of the Immune System. *Comput. Math. Methods Med.* **2012**, *2012*, 842329.
- (55) Safavi, A.; Kefayat, A.; Mahdevar, E.; Abiri, A.; Ghahremani, F. Exploring the out of sight antigens of SARS-CoV-2 to design a candidate multi-epitope vaccine by utilizing immunoinformatics approaches. *Vaccine* **2020**, *38* (48), 7612–7628.
- (56) Duthie, M. S.; Windish, H. P.; Fox, C. B.; Reed, S. G. Use of defined TLR ligands as adjuvants within human vaccines. *Immunol. Rev.* **2011**, *239*, 178–196.
- (57) Forstneric, V.; Ivicak-Kocjan, K.; Plaper, T.; Jerala, R.; Bencina, M. The role of the C-terminal D0 domain of flagellin in activation of Toll like receptor 5. *PLoS Pathog.* **2017**, *13* (8), e1006574.
- (58) Safavi, A.; Kefayat, A.; Abiri, A.; Mahdevar, E.; Behnia, A. H.; Ghahremani, F. In silico analysis of transmembrane protein 31 (TMEM31) antigen to design novel multiepitope peptide and DNA cancer vaccines against melanoma. *Mol. Immunol.* **2019**, *112*, 93–102.
- (59) Safavi, A.; Kefayat, A.; Sotoodehnejadnematalahi, F.; Salehi, M.; Modarressi, M. H. In Silico Analysis of Synaptosomal Complex Protein 1 (SYCP1) and Acrosin Binding Protein (ACRBP) Antigens to Design Novel Multiepitope Peptide Cancer Vaccine Against Breast Cancer. *Int. J. Pept. Res. Ther.* **2019**, *25* (4), 1343–1359.
- (60) Mahdevar, E.; Safavi, A.; Abiri, A.; Kefayat, A.; Hejazi, S. H.; Miresmailei, S. M.; Iranpur Mobarakeh, V. Exploring the cancer-testis antigen BORIS to design a novel multi-epitope vaccine against breast cancer based on immunoinformatics approaches. *J. Biomol. Struct. Dyn.* **2021**, *1*–18.
- (61) Yang, J. Y.; Zhang, Y. I-TASSER server: new development for protein structure and function predictions. *Nucleic Acids Res.* **2015**, *43* (W1), W174–W181.
- (62) Wiederstein, M.; Sippl, M. J. ProSA-web: interactive web service for the recognition of errors in three-dimensional structures of proteins. *Nucleic Acids Res.* **2007**, *35*, W407–W410.
- (63) Rahman, M. M.; Puspo, J. A.; Adib, A. A.; Hossain, M. E.; Alam, M. M.; Sultana, S.; Islam, A.; Klena, J. D.; Montgomery, J. M.; Satter, S. M.; Shirin, T.; Rahman, M. Z. An Immunoinformatics Prediction of Novel Multi-Epitope Vaccines Candidate Against Surface Antigens of Nipah Virus. *Int. J. Pept. Res. Ther.* **2022**, *28* (4), 123.
- (64) Almansour, N. M. Immunoinformatics- and Bioinformatics-Assisted Computational Designing of a Novel Multiepitopes Vaccine Against Cancer-Causing Merkel Cell Polyomavirus. *Front Microbiol* **2022**, *13*, 929669.
- (65) Jacchieri, S. G.; Torquato, R.; Brentani, R. R. Structural study of binding of flagellin by Toll-like receptor 5. *J. Bacteriol.* **2003**, *185* (14), 4243–4247.
- (66) Karplus, M.; Kuriyan, J. Molecular dynamics and protein function. *Proc. Natl. Acad. Sci. U. S. A.* **2005**, *102* (19), 6679–85.
- (67) Vangone, A.; Oliva, R.; Cavallo, L. CONS-COCOMAPS: a novel tool to measure and visualize the conservation of inter-residue contacts in multiple docking solutions. *Bmc Bioinformatics* **2012**, *13*, S19.
- (68) Vangone, A.; Spinelli, R.; Scarano, V.; Cavallo, L.; Oliva, R. COCOMAPS: a web application to analyze and visualize contacts at the interface of biomolecular complexes. *Bioinformatics* **2011**, *27* (20), 2915–2916.
- (69) Abdel-Azeim, S.; Chermak, E.; Vangone, A.; Oliva, R.; Cavallo, L. MDcons: Intermolecular contact maps as a tool to analyze the interface of protein complexes from molecular dynamics trajectories. *Bmc Bioinformatics* **2014**, *15*, S1.
- (70) Mugunthan, S. P.; Harish, M. C. Multi-epitope-Based Vaccine Designed by Targeting Cytoadherence Proteins of *Mycoplasma gallisepticum*. *Acs Omega* **2021**, *6* (21), 13742–13755.
- (71) Mayahi, V.; Esmaelizad, M.; Ganjalikhany, M. R. Development of Avian Avulavirus 1 Epitope-Based Vaccine Pattern Based on Epitope Prediction and Molecular Docking Analysis: An Immunoinformatic Approach. *Int. J. Pept. Res. Ther.* **2020**, *26* (3), 1513–1522.
- (72) Joshi, A.; Pathak, D. C.; Mannan, M. A.; Kaushik, V. In-silico designing of epitope-based vaccine against the seven banded grouper nervous necrosis virus affecting fish species. *Netw Model Anal Health Inform Bioinform* **2021**, *10* (1), 37.
- (73) Zhu, A.; Wei, L.; Hu, S.; Yang, C.; Chen, C.; Zhou, Z.; Pan, Z. Characterisation and functional analysis of canine TLR5. *Innate Immun* **2020**, *26* (6), 451–458.
- (74) Zhu, S. L.; Feng, Y.; Rao, P. H.; Xue, X. Y.; Chen, S.; Li, W. S.; Zhu, G. B.; Zhang, L. F. Hepatitis B virus surface antigen as delivery vector can enhance *Chlamydia trachomatis* MOMP multi-epitope immune response in mice. *Appl. Microbiol. Biot.* **2014**, *98* (9), 4107–4117.